Dynamic Micromagnetic Write Head Fields During Magnetic Recording in Granular Media

Thomas Schrefl, Manfred E. Schabes, Dieter Suess, and Martin Stehno

***Abstract*—Magnetic recording at fast data rates requires write heads with rapid rise times of the magnetic flux during the write process. We present three-dimensional (3-D) micromagnetic finite-element (FEM) calculations of an entire ring head (including 3-D coil geometry) during the writing of magnetic bits in granular media. The calculation of the obtainable flux rise times takes into account the current rise in the coils, the magnetization processes in the yoke, the magnetization processes in the pole regions near the gap, as well as the magnetization dynamics in the magnetic recording media. The simulations demonstrate how input current profiles translate into magnetization processes in the head and media during writing.**

***Index Terms*—Magnetic recording, micromagnetics, ring head.**

I. Introduction

ULTRAHIGH DENSITY magnetic recording requires recording write heads that yield both a high field to overcome the coercivity of the data layer and a high-field gradient in the down-track direction. Optimization of the recording performance goes hand in hand with simulations techniques for an accurate computation of the head fields. Traditionally, head fields are calculated using three-dimensional (3-D) nonlinear eddy current finite-element codes [1]. An alternative approach is the application of finite-integration techniques [2]. Both methods give head fields in agreement with the experiment. With increasing recording densities, the gap decreases. Consequently, a very fine finite-element mesh is required in and below the gap. Park *et al.*[3] proposed a two-step analysis to improve the calculation of the field gradient. They apply a conventional finite-element method to treat the gap region and a Laplacian analysis method to compute the field gradient below the gap.

Magnetic recording at fast data rates requires write heads with rapid rise times of the magnetic flux during the write process. However, a detailed understanding of the physics that determines the obtainable flux rise times is difficult because it requires linking the record current rise in the coils with the magnetization processes in the relatively large yoke and the much smaller pole regions near the gap as well as the magnetization dynamics in the magnetic recording media grains.

In this paper, we report initial results of 3-D micromagnetic finite-element (FEM) calculations of an entire ring head (including 3-D coil geometry) during the writing of magnetic bits in granular media. The magnetization processes in the yoke and gap regions are treated by a micromagnetic hybrid FEM/boundary element method method for solving the LLG equation. Within the framework of this method [4] the finite-element method is used to compute the magnetization and the magnetic field within the head and the media grains. The boundary element method is used to treat the mutual interactions between coil, head, and media. The hybrid FEM/BEM method is an excellent method to bridge the different length scales involved in the simulations. No mesh is required outside the ferromagnetic parts. The head field can be computed accurately, as problems associated with meshing the air gap can be avoided. Section II of the paper briefly introduces the simulation method, and Section III presents computed flux rise times.

II. Micromagnetic and Numerical Background

A. Magnetization Dynamics

The Landau–Lifshitz Gilbert equation [5] is the starting point for dynamic micromagnetic simulations

$$\frac{\partial \boldsymbol{J}}{\partial t} = -|\gamma|\,\boldsymbol{J}\times\boldsymbol{H}_{\mathrm{eff}} + \frac{\alpha}{J_{\mathrm{s}}}\boldsymbol{J}\times\frac{\partial \boldsymbol{J}}{\partial t}. \tag{1}$$

Here, $\boldsymbol{J}$ is the magnetic polarization vector, $\boldsymbol{H}_{\mathrm{eff}}$ is the effective field, α is the Gilbert damping constant, and J_{s} is the spontaneous polarization. The total effective field acting on the magnetization is the usual effective field computed from the variational derivative of the free energy E, augmented by the magnetic field produced by the coil

$$\boldsymbol{H}_{\mathrm{eff}} = \frac{2A}{J_{\mathrm{s}}}\Delta\boldsymbol{u} + \frac{2K_1}{J_{\mathrm{s}}}\boldsymbol{k}(\boldsymbol{u}\cdot\boldsymbol{k}) + \boldsymbol{H}_{\mathbf{ext}} + \boldsymbol{H}_{\mathbf{demag}} + \boldsymbol{H}_{\mathbf{coil}}. \tag{2}$$

Here, $\boldsymbol{u}(\mathbf{x},t)$ is the unit vector of the magnetization as a function of space and time. A is the exchange constant, K_1 is the anisotropy constant, $\boldsymbol{k}$ the unit vector parallel to easy axis, $\boldsymbol{H}_{\mathrm{ext}}$ the external field, $\boldsymbol{H}_{\mathrm{demag}}$ the demagnetizing field, and $\boldsymbol{H}_{\mathrm{coil}}$ the magnetic field produced by the coil.

After space discretization, (1) reduces to a system of ordinary differential equations that can be effectively solved using an adaptive time step backward difference scheme [4]. For the space discretization, the ferromagnetic parts are subdivided into

Manuscript received October 16, 2003. This work was supported by the Austrian Science Fund under Grant Y132-N02.

T. Schrefl and D. Suess are with the Institute of Solid State Phyics, Vienna University of Technology, A-1040 Vienna, Austria (e-mail: thomas.schrefl@tuwien.ac.at; suess@magnet.tuwien.ac.at).

M. E. Schabes is with Hitachi Global Storage Technologies, Hitachi San Jose Research Center, San Jose, CA 95193 USA (e-mail: manfred.schabes@hgst.com).

M. Stehno is with Department of Physics, University of Illinois–Urbana-Champaign, Urbana, IL 61801 USA (e-mail: stehno@mrlnt6.mrl.uiuc.edu).

Digital Object Identifier 10.1109/TMAG.2004.832467

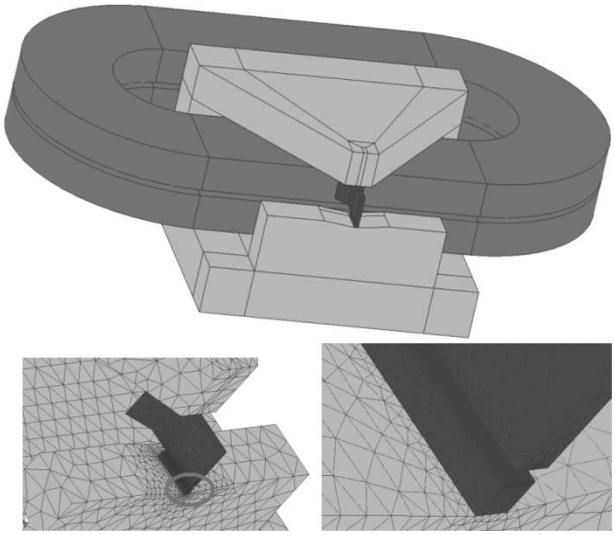

Fig. 1. (Top) Geometry of the coil and the head. The distance between the pole tips is 80 nm. (Bottom) Details of the finite-element mesh in the gap region. The mesh near the surface of the pole tip has a resolution of 5 nm.

tetrahedral finite elements. Then, the effective field can be computed by

$$\boldsymbol{H}_{\mathrm{eff},i} = -\left(\frac{\delta E}{\delta \mathbf{J}}\right)_i = \frac{1}{m_i}\frac{\partial E}{\partial \mathbf{u}_i} \tag{3}$$

where m_i denotes the magnetic moment associated with the node point i.

Using (1)–(3), the magnetization in the head and in the data layer are computed. Eddy currents are not explicitly taken into account in a traditional micromagnetic approach. Eddy currents will give rise to dissipation, leading to an increase of the effective Gilbert damping constant [5].

B. Treatment of the Coil

The field from the current carrying coils is calculated using a boundary integration technique. The current is assumed to be uniform across the cross section of the coil. The field of a polyhedral conductor with uniform current density $\boldsymbol{j}$ can be computed by an integral over its surface [6]. Thus, we obtain

$$\boldsymbol{H}_{\mathrm{coil}} = \frac{1}{4\pi}\int_{\partial\Omega}\frac{\boldsymbol{j}\times\boldsymbol{n}}{|\boldsymbol{r}-\boldsymbol{r}'|}dA \tag{4}$$

where the integration is over the surface of the coil. $\boldsymbol{j}$ is the current density, and $\boldsymbol{n}$ is the normal vector at the surface. In our micromagnetic simulations, the surfaces of the pancake-shaped conductors of the coil (see Fig. 1) are subdivided into triangles. Each surface triangle contributes to $\boldsymbol{H}_{\mathrm{coil}}$. The corresponding surface integrals are computed analytically [7]. $\boldsymbol{H}_{\mathrm{coil}}$ has to be computed on the nodes of the finite-element mesh of the head. The discretization of the surface integral (4) can be written as matrix vector product. The interaction matrix is fully populated and relates the surface triangles of the coil with the nodes of the head. In order to save memory and to speed up the matrix vector product, we apply a matrix compression technique based on the adaptive cross-approximation method [8].

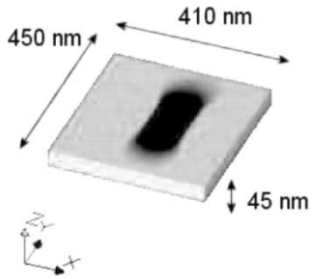

Fig. 2. Head field is computed in a box below the gap region. Here, the color code denotes the H_{x} component of the head field 10 nm below the gap. The pole tips of the head are fully saturated.

Fig. 1 shows the geometry of the coil and the ring head. The surface of the coil is subdivided into surface triangles. The yoke and the pole tips are meshed using tetrahedral finite elements.

C. Magnetostatic Self-Interaction

A hybrid finite-element boundary element method is used for the calculation of the demagnetizing field [4]. Instead of computing the demagnetizing field directly, we solve the magnetostatic boundary value problem for a magnetic scalar potential and compute the field from the gradient of the potential. The open boundary problem is treated using a fast boundary element method as outlined in [9].

D. Head-to-Media Interaction/Media to Head Interaction

Within the framework of the FEM/BEM method, we compute the magnetic scalar potential to treat the magnetostatic interaction of distinct magnetic parts [9]. For example, the scalar potential produced by the head magnetization follows from a surface integral over the surface of the head. Again, these integrals can be calculated analytically for each surface triangle [7]. In order to compute the head field in the recording layer, we evaluate the potential of the head at the surface of a "field box" with an extension of $450 \times 410 \times 45$ nm^3 (shown in Fig. 2). Then a fast Poisson solver is used to compute the potential from the head within the field box at a high spatial resolution. Numerical derivation gives the head field. Fig. 2 shows the field box used for the simulations. Again, we use matrix compression techniques to reduce the size of the interaction matrix, which relates the surface nodes of the head with the surface nodes of the field box. The media-to-head interactions are handled in a similar way.

III. Results

Head fields were calculated for the ring head shown in Fig. 1. The saturation polarization J_{s} was 2 T in the yoke and 2.4 T in the gap region. The coil is modeled by two conductor bars with a cross section area of 6.2 $(\mu\mathrm{m})^2$. The maximum applied current is $I_{\max} = 120$ mA. In order to account for eddy current effects, we use a Gilbert damping constant $\alpha = 0.1$ for the head, instead of the low intrinsic damping constant of NiFeCo. The driving current changes $+I_{\max}$ to $-I_{\max}$ in a time of 0.2 ns.

The obtainable flux rise time is calculated with the following procedure. First, we calculate the dynamic magnetization processes in the head for two periods of the driving current. For

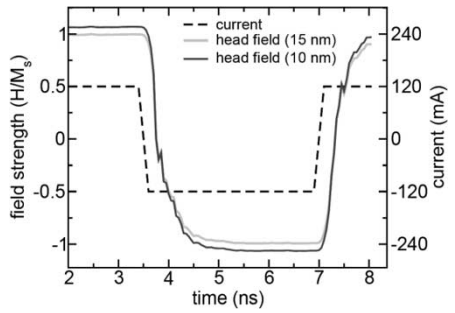

Fig. 3. Write field strength as a function of time. The dashed line gives the write current profile. The green line and the red line give the magnitude of the head field 15 and 10 nm below the gap, respectively.

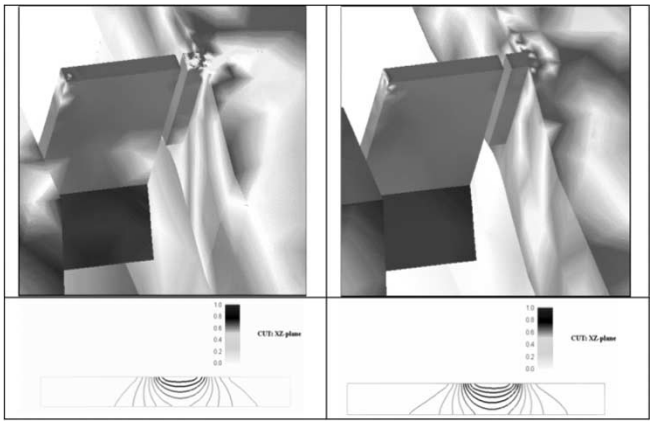

Fig. 4. Increase of the head field as a function of time. (Top) The down-track component of the magnetization is color coded in the gap region of the head. (Bottom) The magnitude of the head field in units of M_s in a slice through the media parallel to the down-track direction. (Left) 0.05 ns after reversing the current. (Right) 1.15 ns after reversing the current.

the third period, we also calculate the head field. Fig. 3 shows the driving current and the head field strength. The maximum head field is reached 2 ns after the reversing the current. This delay can be understood by the dynamic magnetization processes within the head. Fig. 4 gives the magnetization in the pole tips at 0.05 and 1.15 ns after reversing the current. The magnetization is color-coded. Only if the pole tips appear completely red is full saturation reached. In addition, Fig. 4 shows the head field within the recording layer. The contour plot gives the field component parallel to the down track at different depth inside the data layer. It takes more than 1 ns for the head field to penetrate sufficiently wide into the data layer.

The simulation method was used to record magnetic transitions. The data layer consists of grains with a diameter of 8 nm and a height of 12 nm ($J_s = 0.5$ T, $K_1 = 2.4 \times 10^5$ J/m^3, $A = 10^{-11}$ J/m). The grains are weakly exchange coupled through a 1–nm-thick boundary phase with an exchange constant of $A = 3 \times 10^{-14}$ J/m. The easy axes of the grains are randomly oriented in plane. In order to reduce the number of degrees of freedom, each grain is treated as a single domain particle. The total number of degrees of freedom is about 50 000. The CPU time required to simulate the write process for a time of 21 ns is 4.5 h on an alpha processor with 1 GHz. Initially, the pole tips of the head were demagnetized. The head was placed above the dc demagnetized data layer with a head-to-media distance of 10 nm. Fig. 5 gives the magnetization in the data layer after writing four transitions.

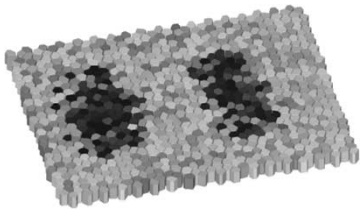

Fig. 5. Three-dimensional view of the data layer after recording four transitions. The grayscale maps the magnetization parallel to the down-track direction. The head velocity was 10 m/s.

IV. Conclusion

Novel numerical techniques for fully integrated magnetic recording simulations are presented. The method accurately handles the mutual interactions between the coil, head, and media. The method was used to compute the obtainable flux rise time during magnetic recording in granular media.

References

[1] Y. Kanai, R. Matsubara, K. Fujiwara, and N. Takahashi, "New structured planar write head for 100 Gb/in^2 and beyond," *IEEE Trans. Magn.*, vol. 38, pp. 2210–2212, Sept. 2002.

[2] M. Clemens, S. Drobny, and T. Weiland, "Numerical analysis of a magnetic recording write head benchmark problem using the finite integration technique," *IEEE Trans. Magn.*, vol. 38, pp. 601–604, Mar. 2002.

[3] G. S. Park, H. Won, K. C. Kim, and J. D. Suh, "Design of the recording head considering the field gradient in high density magnetic recording," in *Proc. 14th Compumag Conf. Computation of Electromagnetic Fields*, vol. II, Saratoga Springs, NY, July 2003, pp. 38–39.

[4] D. Suess, V. Tsiantos, T. Schrefl, J. Fidler, W. Scholz, H. Forster, R. Dittrich, and J. Miles, "Time resolved micromagnetics using a preconditioned finite element," *J. Magn. Magn. Mater.*, vol. 248, pp. 298–311, 2002.

[5] S. Chikazumi, *Physics of Ferromagnetism*, 2nd ed. Oxford: Clarendon, 1997, pp. 562–567.

[6] M. Gyimesi, D. Lavers, T. Pawlak, and D. Ostergaard, "Biot-Savart integration for bars and arcs," *IEEE Trans. Magn.*, vol. 29, pp. 2389–2391, Nov. 1993.

[7] D. A. Lindholm, "Three-dimensional magnetostatic field from point matched integral equations with linearly varying scalar sources," *IEEE Trans. Magn.*, vol. 20, pp. 2025–2032, Sept. 1984.

[8] S. Kurz, O. Rain, and S. Rjasanow, "The adaptive cross-approximation technique for the 3D boundary-element method," *IEEE Trans. Magn.*, vol. 38, pp. 421–424, Mar. 2002.

[9] H. Forster, T. Schrefl, R. Dittrich, W. Scholz, and J. Fidler, "Fast boundary methods for magnetostatic interactions in micromagnetics," *IEEE Trans. Magn.*, vol. 39, pp. 2513–2515, Sept. 2003.